The X-ray Microcalorimeter Spectrometer onboard of IXO

J.W. den Herder[a], R.L. Kelley[b], K. Mitsuda[c], L. Piro[d], S.R. Bandler[b], P. Bastia[g], K.R. Boyce[b], M. Bruin[a], J.A. Chervenak[b], L. Colasanti[d], W.B. Doriese[m], M. DiPirro[b], M.E. Eckart[b], Y. Ezoe[j], E.Figueroa-Feliciano[k], L. Ferrari[b], R. Fujimoto[i] ,F. Gatti[e], K.C. Gendreau[b], L. Gottardi[a], R. den Hartog[a], G.C. Hilton[b], H. Hoevers[a], K.D. Irwin[m], Y. Ishisaki[j], A. Kashani[n], C.A. Kilbourne[b], P. de Korte[a], J. van der Kuur[a], C.Macculi[d], T. Mineo[h], J.H. Nieland[a], T. Ohashi[j], S. Paltani[o], E Perinati[h], F.S. Porter[b], P.J. Shirron[b], S.J. Smith[b], Y. Takei[c], M. Tashiro[l], G. Torrioli[f] , M. Tsujimoto[c], H. van Weers[a], N.Y. Yamasaki[c]

[a] *SRON, Netherlands Institute for Space Research, Sorbonnelaan 2, 3854 CA Utrecht*
[b] *NASA/Goddard Space Flight Center, Greenbelt, MD 20771, USA*
[c] *Institute of Space and Astronautical Science, 3-1-1 Yoshinodai, Sagamihara, Kanagawa 229-8510, Japan*
[d] *INAF/IASF-Roma, Via del Fosso del Cavaliere, 100, 00133, Roma, Italy*
[e] *INFN-Physics, Department Genova University, Via Dodecameso 33, 16146 Genova, Italy*
[f] *IFN, CNr-Roma, IFN-CNR, Via Cineto Romano 42, 00156 Roma, Italy*
[g] *Thales Alenia Space Italia S.p.A. S.S. Padana Superiore 290, 200900 Vimodrone, Milano, Italy*
[h] *INAF-IASF Palermo, Via Ugo La Malfa 153 90123 Palermo, Italy*
[i] *Faculty of Mathematics and Physics, Kanazawa University, Kakuma-machi, Kanazawa, Ishikawa 920-1192, Japan*
[j] *Tokyo Metropolitan University, 1-1 Minami-Osawa, Hachioji, Tokyo 192-0397, Japan*
[k] *MIT, Kavli Institute for Astrophysics and Space Research, Massachusetts Institute of Technology, 70 Vassar Street, Cambridge, MA 02139, USA*
[l] *Saitama University, School of Science and Engineering, 255 Shimo-Okubo, Sakura-ku, Saitama City, Saitama 338-8570, JAPAN*
[m] *NIST, National Institute of Standards and Technology, Mail Stop 814. 03325 Broadway, Boulder, CO 8030, USA*
[n] *Atlas Scientific, NASA-ARC, M/S 244-10, Moffett Field, CA 94035-1000, USA*
[o] *ISDC, University of Geneva, ch. d'Écogia 16, CH-1290 Versoix, Switzerland*

ABSTRACT

One of the instruments on the International X-ray Observatory (IXO), under study with NASA, ESA and JAXA, is the X-ray Microcalorimeter Spectrometer (XMS). This instrument, which will provide high spectral resolution images, is based on X-ray micro-calorimeters with Transition Edge Sensor (TES) with absorbers that consist of metal and semi-metal layers and a multiplexed SQUID readout. The requirements for this instrument are demanding. In the central array (40 x 40 pixels) an energy resolution of < 2.5 eV is required, whereas the energy resolution of the outer array is more relaxed (≈ 10 eV) but the detection elements have to be a factor 16 larger in order to keep the number of read-out channels acceptable for a cryogenic instrument. Due to the large collection area of the IXO optics, the XMS instrument must be capable of processing high counting rates, while maintaining the spectral resolution and a low deadtime. In addition, an anti-coincidence detector is required to suppress the particle-induced background.

In this paper we will summarize the instrument status and performance. We will describe the results of design studies for the focal plane assembly and the cooling systems. Also the system and its required spacecraft resources will be given.

Keywords: X-ray, missions, micro-calorimeter, International X-ray Observatory

Space Telescopes and Instrumentation 2010: Ultraviolet to Gamma Ray,
edited by Monique Arnaud, Stephen S. Murray, Tadayuki Takahashi, Proc. of SPIE Vol. 7732,
77321H · © 2010 SPIE · CCC code: 0277-786X/10/$18 · doi: 10.1117/12.856018

1. INSTRUMENT REQUIREMENTS

The specific instrument requirements are derived from the top level requirements for the IXO mission [1]. The XMS instrument will provide the capability to fully exploit the large area and high angular resolution of IXO by combining this with a similar improvement in imaging spectral resolution. The key instrument requirements are listed in table 1.

Table 1: Main instrument requirements

Parameter	Requirement	Comment
Inner array		
Energy range	0.3 – 12 keV	Goal: 0.1 – 12 keV
Energy resolution: E < 7 keV E > 7 keV	2.5 eV E/ΔE = 2800	
FoV	2 arcmin	Corresponds to 40 x 40 pixels
Pixel size	300 μm	
good grade events	50 counts/sec/pixel	> 80% of the events will provide the 2.5 eV resolution
Outer array		
Energy range	0.3 – 12 keV	Goal: 0.1 – 12 keV
Energy resolution: E < 7 keV E > 7 keV	10 eV E/ΔE = 700	
FoV	5.4 arcmin	Corresponds to a detector size of 31.2 x 31.2 mm^2
Pixel size	600 μm	
good grade events	2 counts/sec/pixel	>80% of the events will provide 10 eV resolution
Full array		
Absolute Time	50 μs	
Time resolution	10 μs	
Quantum efficiency @ 1 keV @ 7 keV	> 60 % > 80 %	Including filters and detector filling factor
Relative uncertainty in QE between pixel	< 3 %	Achieved by calibrations
Energy resolution uniformity (FWHM)	1 eV	Fit by a Gaussian distribution
Effective area change due to contamination over lifetime	< 10 % over 0.2 < E < 1 keV	Depending on the contaminant (water or hydrocarbons)
Non X-ray background	2 10^{-2} counts/cm^2/keV/s	
Continuous observing time	> 31 hour	
Regeneration time	< 10 hr	
Energy scale stability	1 eV / h	

The requirements have been split between an inner array and an outer array. In the inner array the ultimate spectral resolution is required using relatively small pixels of 300 μm (note that the mirror PSF has a HPD of 500 μm). In order to cover the field of view, while keeping the number of pixels and the wiring to the cryogenic detector at a reasonable level, the spectral resolution and the count rate capability of the outer array has been relaxed to 10 eV and 2

counts/s/pixel respectively. The relatively modest energy scale stability requirement will not affect the energy resolution of the instrument as we will monitor the gain on a 10 minute time-scale using the onboard calibration sources.

For a micro calorimeter array the fraction of events with the highest spectral resolution depends on the countrate of the incident photons. This is illustrated in figure 1 where an example is given of different categories of x-rays according to the relative timing of x-ray events. The high resolution will be achieved only if the time since the previous photon is large enough and if during the time following the observed photon the detector element is not hit by another photon (top panel). The simulations in figure 1 (right side) assume 10 τ and 40 τ, for the time before and after the selected event. With τ = 0.187 ms this results in a free record length of about 4.5 ms, thereby enabling 80% high-resolution events for an input countrate of 50 c/s/pixel.. Using appropriate filtering the mid-res events typically have a resolution of 3.5 eV which is still very good. In figure 1 the fraction of high-res, mid-res and low-res events at a specific countrate is given. For observations with high count rates one can of course select only the outer part of the PSF where the countrate per pixel is below the specified levels or one can insert a so-called beam diffuser in front of the detector. This is a small curved micro channel plate which diffuses the beam over a small circular ring on the detector (hence spreading the flux over more pixels). The disadvantages of this approach are that the reflectivity of the beam diffuser is less than 1 and that the reflectivity is energy dependent.

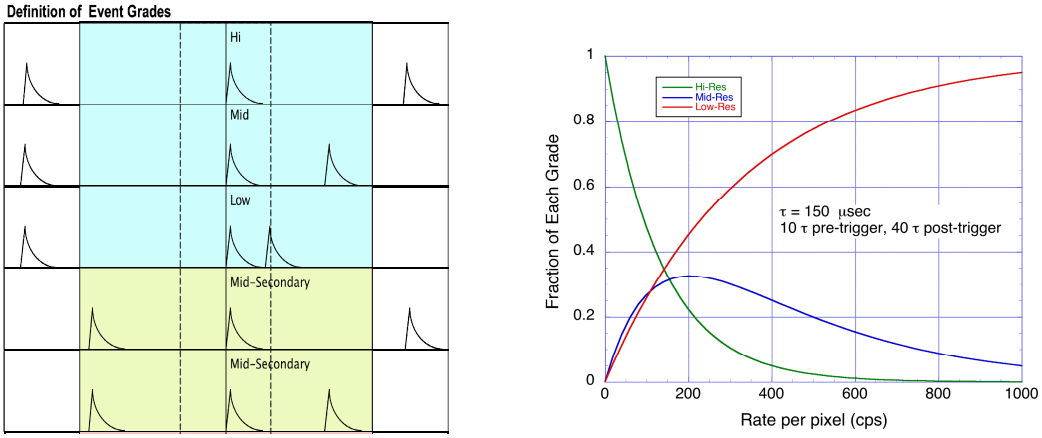

Figure 1: Definition of event grades for a calorimeter and distribution of high-res, mid-res and low-res events as function of countrate per pixel

2. FOCAL PLANE ASSEMBLY DESIGN

The design of the FPA is a major challenge as it has to meet a large number of requirements. The most important are:

- The performance critical design parameters of the TES-detector arrays include: a heat capacitance of 0.8 pJ/K for the inner array and 10.8 pJ/K for the outer array, thereby allowing for an absorber thickness (1 μm Au and 4 μm Bi) to provide sufficient stopping power at 7 keV; a Mo/Au bilayer Transition Edge Sensor with a T_C of 70 (outer) and 90 (inner) mK with a temperature coefficient α_I = 75, and a current coefficient β_I = 1.25. The typical bias point for this TES is 1 mΩ. Furthermore the pixel support structures should be optimized for heat sinking to reduce crosstalk in the array and to reduce the influence of cosmic rays. The intrinsic energy resolution (no read-out contributions) for this detector (inner array) is 1.7 eV. Including the contributions due to the multiplexing noise (TDM-limited) and the finite record length (countrate limited) raises the energy resolution to 2.3 eV. The difference with the required 2.5 eV is just enough to cover all other contributions (temperature stability, gain variations, thermal and electrical cross talk, etc).

- For the outer array the pixel area has been increased by a factor 4 (from 300 μm squared pixels to 600 mm squared). In addition 4 pixels are connected to a single TES with a different thermal coupling, allowing the onboard processing software to discriminate between these thermal couplings [2]. This results in an energy resolution of about 10 eV.

- To reject charged particles an anti-coincidence detector is required just underneath the detector proper. As a baseline we have chosen a Si-based detector that is between 0.3 and 0.5 mm in thickness. Using the athermal component of the phonon response, the anti-coincidence detector will be very fast ($\tau_{rise} < 30$ μs, $\tau_{fall} < 300$ μs), so that the timing is accurate enough to reject coincident events in the pixel array. The Si-based AC will also be read-out by a TES. The chosen geometry (oversize with respect to the array) and the energy discrimination of TES-pixels will give a rejection efficiency of > 0.99 for ionizing particles. Most of the remaining background will be secondaries.

- The heat load of the detector has to be low at the 50 mK level. This requires low power dissipation of the electronic components at this temperature and multiplexing of the detector signals at the 50 mK level to keep the wiring to an acceptable low level. For the multiplexing we have selected time domain multiplexing in which up to 32 pixels in a single column are read-out sequentially. Potentially more powerful read-out schemes such as frequency domain multiplexing and code division multiplexing are under development, but have not yet shown the required performance.

- The temperature of the detector should be very well controlled. The detector, which will be operated around 15% of its normal resistance, has to be controlled to within < 1μK rms and a drift of < 5 μK over 10 minutes. (changes due to variations at a scale > 10 minutes will be monitored and corrected using the onboard calibration source).

- A very low magnetic field at the position of the detector: the static B-field at the TES and SQUID should be < 1 μT during cool down and any field drifts should be < 140 pT over 10 minute time-scale. This can only be achieved with proper control of the magnetic field outside the detector and shielding of the last stage cooler. Our current design of magnetic shielding of the detector itself includes a cryoperm shield at 4 K and a superconducting Nb shield at 50 mK. Special consideration has been given to the open slots in this shield (not just for the entrance window but also for the harness and connections to the cold temperature stages) as these can potentially reduce the shielding efficiency. This is shown in figure 5 where the calculated magnetic field for the focal plane assembly is shown.

- The focal plane assembly requires two optical blocking filters to reject the thermal and IR load on the detector. One is mounted at the 50 mK level and the other at the intermediate temperature level.

- The focal plane assembly needs to be compact and modular. In our design we have kept the focal plane assembly volume within a 20 cm diameter and a height of 25 cm using only technology with significant flight heritage (e.g. wire bonding). The total mass of the focal plane assembly is 2.2 kg.

In figure 2 we show the detector layout indicating the split between the inner and the outer array. In figure 3 we show the focal plane assembly including all its components and in figure 4 we zoom in on the detector proper, clearly showing the stacking of the outer array, the inner array and anti-coincidence detector. In figure 5 the calculated magnetic shielding is shown.

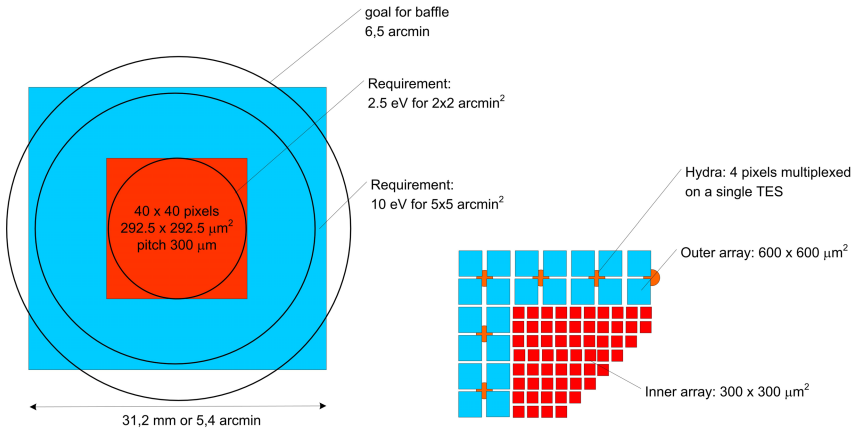

Figure 2. Layout of the focal plane with the inner array (red) with 2.5 eV an the outer array (cyan) with 10 eV resolution. The pixels in the outer array are larger and four pixels are thermally connected to a single TES.

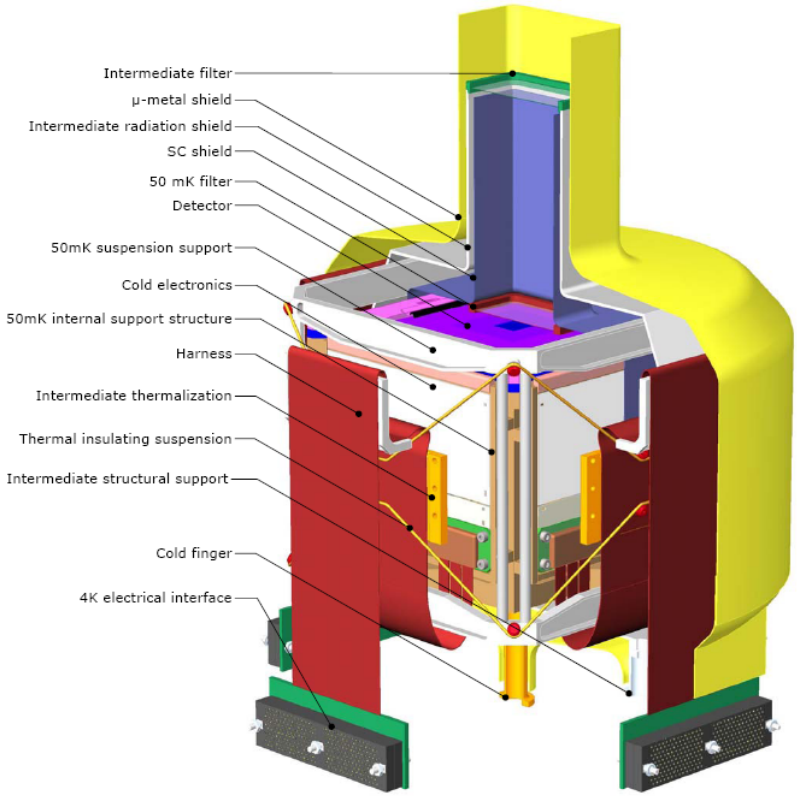

Figure 3. 3D design drawing of the focal plane assembly. The outer shield is at 4 K. Between the detector, which is at 50 mK and the outer shield there is an intermediate radiation shield at 0.3 to 0.6 K (gray). The temperature stage is also used to thermally anchor the wiring. The electronics (SQUIDs, filters etc) is mounted on the side walls of the focal plane assembly to enable a compact design.

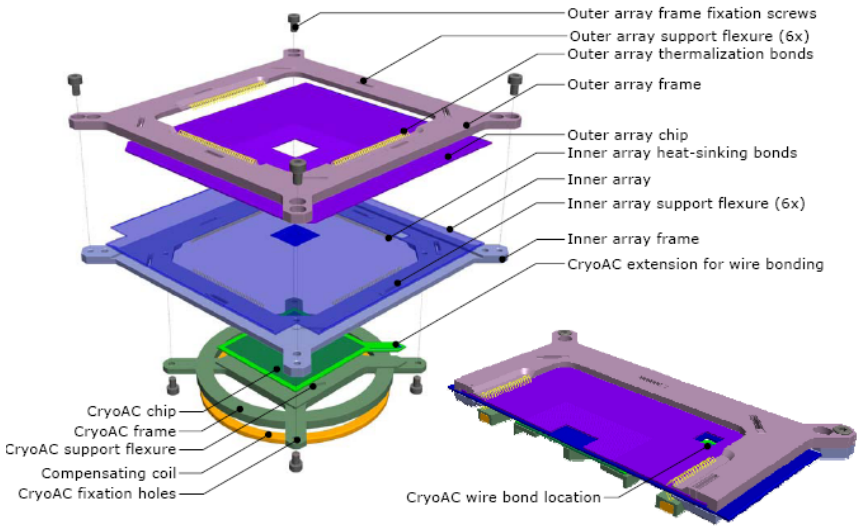

Figure 4. Exploded view of the detector assembly with the outer array, the inner array and the anti-coincidence detector.

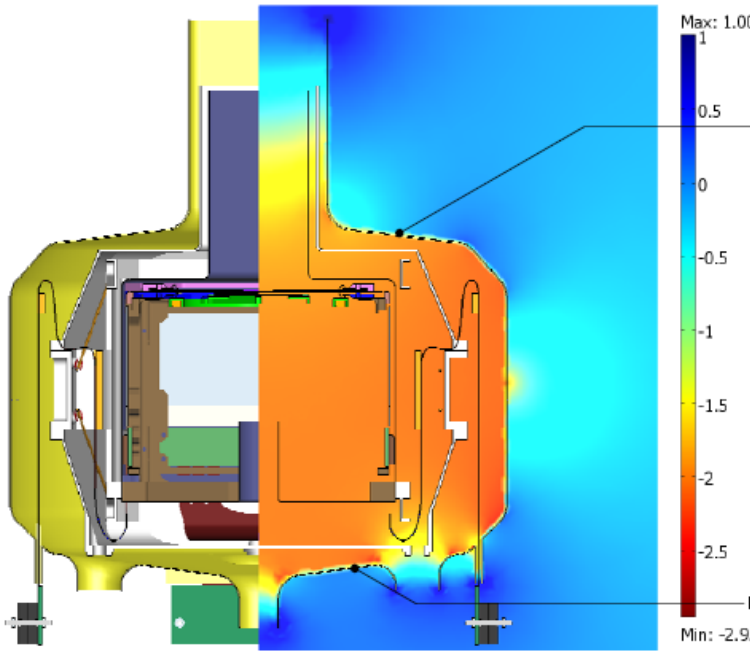

Figure 5. Calculated magnetic fields in the vicinity of the detector and read-out electronics (log scale for the μ-metal shield). Clearly visible is the effect of the open aperture and extended snout on the fields witin the focal plane assembly. At the position of the detector the magnetic field suppression is $10^{-2.}$. Together with the 6 10^{-4} for the superconducting shield this gives a total suppression by a factor 6 10^{-6}.

3. COOLING CHAIN

The cooling chain can be split into two major components: the last stage cooler which cools to 50 mK from a temperature that is between 2 and 4 K and the rest of the cooling chain that provides the cooling power to this 2 - 4 K stage. The last stage cooler can be cycled at regular intervals, allowing for regeneration, whereas the cooling chain from room temperature has to provide continuous cooling.

3.1 50 mK cooler

There are a wide variety of technologies that are able achieve the required low temperature of 50 mK starting from between 2 and 4 K. These systems all do require an intermediate temperature at which the harness can be thermally anchored. All these systems have to meet the necessary cooling requirements. These include: the cooling power at 50 mK (3.0 μW if the intermediate stage is at 0.3 K); the stability of the temperature (1 μK rms, 5 μK drift); operational life (> 5 years implying a cryogenic free system), heat load to the heat bath (20 mW at 2 or 4 K); hold and regeneration time (31 hours and < 10 hours for regeneration), and magnetic shielding. We have selected as baseline a 3 stage ADR which cools down from 4K based because of its maturity (it will be flown on the Astro-H mission) [3]. A schematic diagram of this cooler is shown in figure 6 and a realistic drawing including the dimensions is shown in figure 7. The system is based on a CPA salt pill for the first stage and 2 GLF salt pills for the 2nd and 3rd stage. Its total mass, including magnetic shielding, is 13.3 kg.

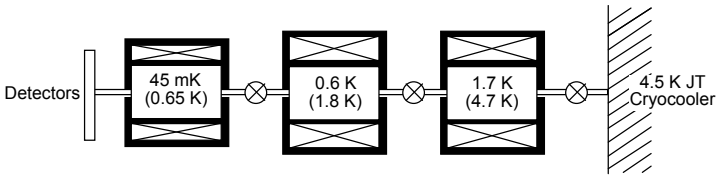

Figure 6 Schematics of the 3 stage ADR selected as baseline for the XMS last stage cooler from 4 K to 50 mK

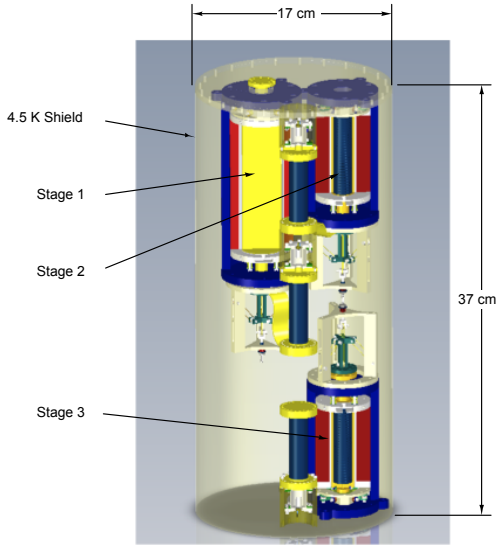

Figure 7 . Realistic drawing of the XMS last stage cooler including relevant dimensions

Other options for the cooling system include systems which prefer an interface temperature at 2 K (double ADR, a combination of a sorption cooler with a single stage ADR, and a closed cycle dilution refrigerator). A 5 stage ADR, which can operate continuously has also been studied and this can also operate from the 4 K level.

3.2 Cooling chain

The cooling from room temperature to the 2-4 K stage can be achieved by existing and proven technology using purely mechanical coolers. These coolers include 2 stage Stirling coolers, 4He Joule Thomson coolers (and possibly also 3He

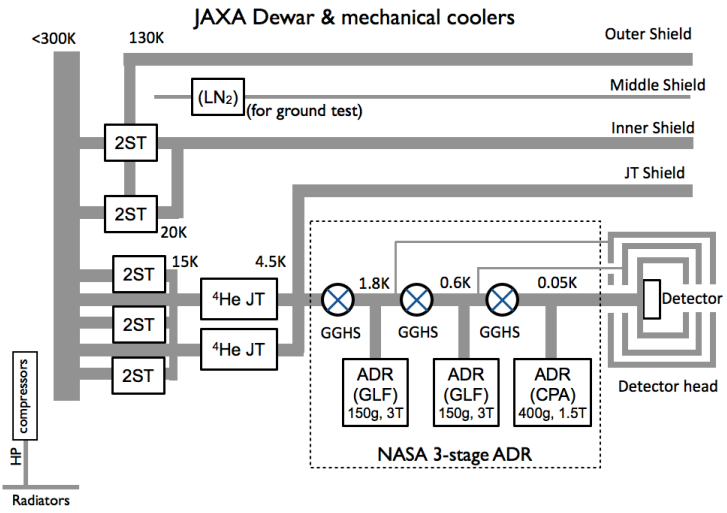

Figure 8 Schematics of the XMS cooling chain. All mechanical coolers are redundant. Details are given by Mitsuda et. al. [4].

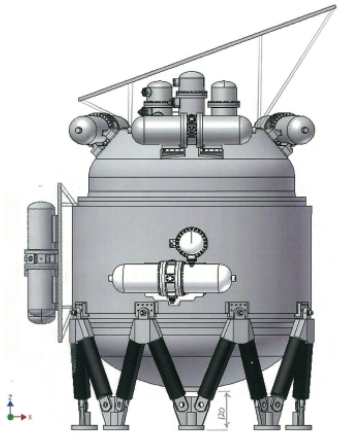

Figure 9. Realistic drawing of the dewar, at the top the radiator is shown.

JT), 3-stage pulse tube cooler, a 4 stage pulse tube cooler and reverse-Brayton cooler in combination with a JT cooler. A key requirement, apart from mass and power, is that the system should be fully redundant in case there is a failure of a single mechanical cooler. It should be noted, however, that many of proposed cooling chains have a very good track record and calculations show already that reliabilities > 0.98 can be achieved without a fully redundant cooling system. As the total cooling system is very complex, we have selected as baseline a system which is based on the cooling system of Astro-H [4]. The schematics is shown in figure 8. Two 2-stage Stirling coolers provide a 20 K temperature shield. These coolers run typically at 50% of their power and if there is a failure in one of them this can be compensated by an increase of the total power to maintain operation. For the same reason we have implemented two ^{4}He JT coolers which are pre-cooled by three 2-stage Stirling coolers. Again, if there is a mechanical failure of a single cooler, the other coolers can take over. Of course, the corresponding electronics is also fully redundant. The LN_2 line, also shown in the figure, allows for relatively fast cooling during ground testing (cool down within 2 weeks instead of in 4 weeks). The mass of the dewar and cryocoolers is about 201 kg, the drive electronics slightly less than 60 kg and the required electrical power is about 540 W. In figure 9 we show the full design of the dewar and its cryocoolers.

4. SYSTEM DESIGN

The system design is shown in figure 10. The front end electronics (FEE) reads-out the detector and is placed in close proximity to the dewar. As the detector is sensitive to EMC, a dedicated and well filtered power supply unit (PSU) is used. The SQUID multiplexer control, the data digitization and the generation of the feedback signals take place in the digital electronic box (DE). This functionality is combined with that of the event processing functionality (EP). The EP includes two major functions: event triggering and pulse height analysis. For practical reasons the DE/EP functionality is split over two separate units. For redundancy the whole signal chain is split in 4 independent quadrants. If there is a failure in one of those, the 3 other quadrants will not be affected. The instrument control unit (ICU) and power distribution unit (PDU) are cold redundant and interface with the satellite. The total mass for the electronic units is 62 kg and 360 W.

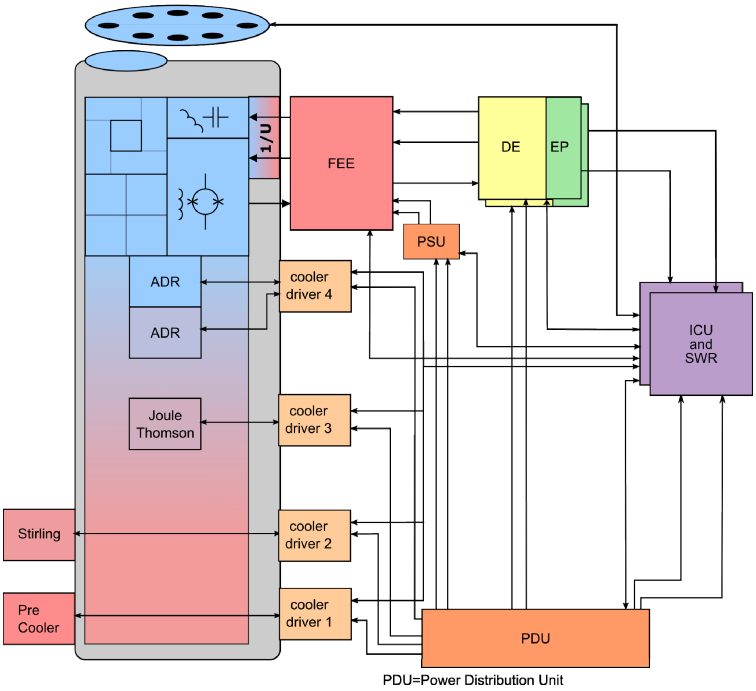

Figure 10.. The X-ray Micro-calorimeter Spectrometer system design.

In addition a filter wheel unit allows filters to be placed in the beam. These will include filters to reduce the optical load on the detector for the observation of bright stars, a beam diffuser for observation of very bright (point) sources and a closed position to protect the detector against micro-meteorites. If, for the closed position, a thick Be filter is selected it can also be used to optimize the number of high-res events at higher energies (> 3-4 keV) at the cost of suppressing the low energy part of the spectrum. Between the focal plane assembly and the ambient environment of the dewar an additional 3 optical blocking filters are required to reduce the thermal load on the detector to reasonable levels. Of course, the cooling chain needs its dedicated drive electronics for the last stage cooler, the shield coolers (two 2-stage Stirling Coolers) and the two ^{4}He JT coolers with the three 2-stage Stirling pre-coolers).

The total mass of the instrument, including a 20% margin, is 409 kg and it requires about 1 kW of power (including a 10% margin). The cool down of the instrument will take about 4 weeks and during operation the regeneration time is < 2 hours whereas the hold time is about 30 hours. The expected telemetry rate is 64 kbit/s (typical) with a maximum of 840 kbit/s (bright sources).

5. CONCLUSIONS

In this paper we have presented the design of the X-ray Micro-calorimeter Spectrometer onboard of IXO. Based upon very conservative selection of technology it is possible to meet the instrument requirements within the given mass, power and volume of the model payload as studied by ESA and NASA. In Figure 11 we show spectra from 16 pixels of an 8x8 array read out using two time-division multiplexer channels. The spectra (obtained using an 55Fe source) are offset for clarity [5]. Fits to the intrinsic line profile are overlaid in blue and red and show an energy resolution of 2.9 eV with high uniformity. These results a already close to the requirement of 2.5 eV. A clear development path has been identified to extend the read-out of 16 channels of an 8 x 8 array into a large set of channels with each 32 detector elements. In figure 12 we show the predicted quantum efficiency of the instrument. It includes a conservative estimate for the optical blocking filters in the dewar, dead space between the detector elements, the thickness of the absorbers, a realistic estimate of the contamination and a certain fraction of pixels which are out of spec after production. The expected energy resolution is also shown. It should be recognized that this is the mean detector resolution and some pixels may deviate from the shown resolution.

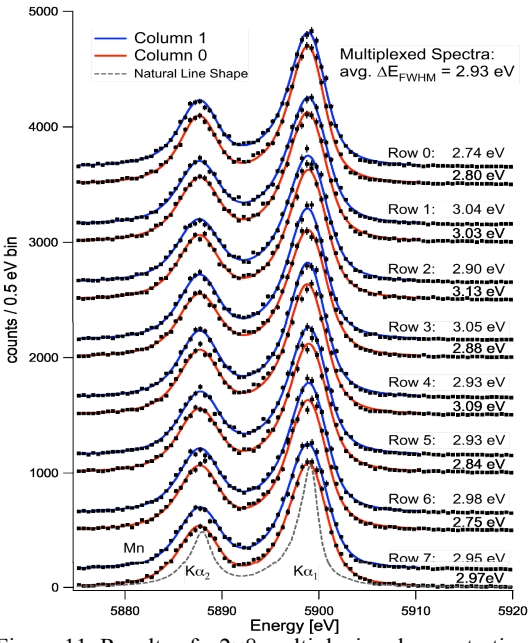

Figure 11. Results of a 2×8 multiplexing demonstration showing 2.9 eV energy resolution using a Goddard array and NIST SQUID multiplexing electronics at NIST. The black points show histograms of manganese (Mn) Kα x-rays from an 55Fe source for each pixel acquired simultaneously, with vertical offsets for clarity and fits to intrinsic line profile overlaid in blue and red. Spectra previously published by Kilbourne, et al. (2008) [5].

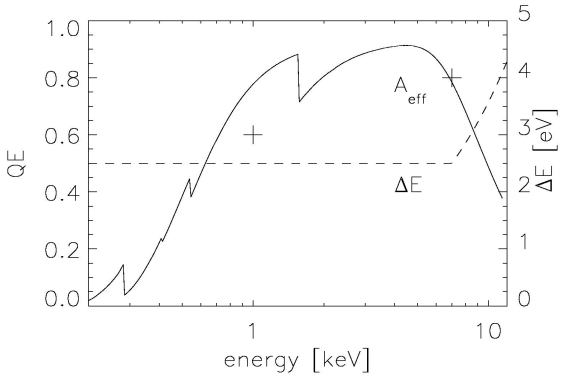

Figure 12. predicted detector quantum efficiency and spectral resolution of the inner array. The IXO top level requirement is shown as two crosses.

REFERENCES

[1] Bookbinder, J, "An overview of the International X-ray Observatory", Proc SPIE 7732-46

[2] Smith S.J. et al., "Development of arrays of position-sensitive micro-calorimeters for Constellation-X", Proc SPIE 7011, 7011-26

[3] Shirron P. et al, "Design of a 3-stage ADR for the soft X-ray spectrometer instrument on the Astro-H mission" Proc SPIE 7732-37

[4] Mitsuda, K et al. "The high resolution X-ray Microcalorimeter Spectrometer system for SXS on Astro-H"", Proc SPIE 7732-36

[5] Kilbourne, C. et al., "Multiplexed read-out of uniform arrays of TES X-ray microcalorimeters suitable for Constellation-X ", Proc SPIE 7011, 701114